# Kinetic Effects in the Scrape Off Layer

R. Chodura
Max-Planck-Institut für Plasmaphysik, EURATOM-IPP Association,
8046 Garching bei München, Germany

## Abstract

The scrape off layer (SOL) of a confined plasma (Fig. 1a) is in many respects in a state far from thermodynamic equilibrium:

- The energy diffusing outward from the plasma core across the separatrix is condensed in the thin SOL to a strong energy flux along the magnetic field.
- The recycling of cold neutrals from the limiter or divertor target gives rise to a strong temperature gradient from the hot midplane region to the relatively cold recycling zone.
- For long mean free path length in the plasma relative to the extension of the recycling zone the thermalization in the recycling zone may be incomplete.
- The potential gradient length in the sheath in front of the target is small as compared to the mean free path length; the velocity distributions of ions and electrons as determined by the electric field are far from being Maxwellians there.

Thus the follwing topics will be discussed in this paper:

- Parallel transport (electron heat flow, ion viscosity)
- Recycling
- Sheath structure (grazing incidence of magnetic field, secondary electrons).
- Boundary conditions for fluid models

Numerical illustrations for these kinetic effects are given from a 1d particle-in-cell code including Coulomb collisions [1].
Not treated are kinetic effects connected with instabilities, perpendicular transport, neutrals and impurities.

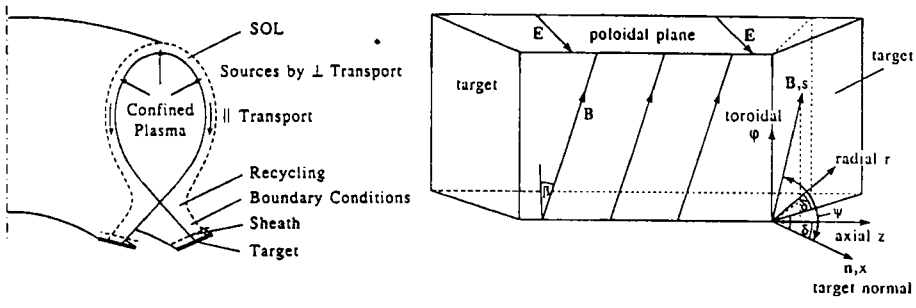


Fig. 1a, b: *Axisymmetric and straightened geometry of the scrape off layer (SOL)*

## 1. Geometry

In studying kinetic effects in the SOL one is interested in basic features in velocity space rather than in an exact modelling of the spatial situation. The higher dimensionality due to inclusion of v-space is achieved on the expense of a simplified geometry in configuration space: The axially symmetric SOL is straightened to a prism limited by two target plates as shown in Fig. 1b. The

magnetic field $\underline{B}$ lies in the toroidal ($\varphi$, z)-plane, the electric potential field $\underline{E}$ and the normal to the target $\underline{n}$ in the poloidal (r,z)-plane. $\delta$ is the angle between target normal and axial (z) direction, $\beta$ the angle between magnetic field and toroidal ($\varphi$) direction, $tg\beta = B_z/B_\varphi = 1/(Aq)$ with aspect ratio A and safety factor $q$. The angle $\psi$ between magnetic field and normal to the target, which is important for the sheath structrure at the target, is given by

$$cos\ \psi = cos\ \delta\ sin\ \beta. \tag{1.1}$$

By using a straight geometry neo classical effects in the SOL are ignored. In the following kinetic effects are treated either along $\underline{B}$ (coordinate s, parallel transport) or along $\underline{n}$ (coordinate x, sheath).

## 2. Electron Heat Flow along B in the SOL

Electron heat flow from a region of the SOl adjacent to the plasma core along the magnetic field to the target plates is a major energy loss channel of the confined plasma. It is, therefore, worthwhile to study this energy transport in more detail.

### 2.1 Local Electron Heat Conduction Theory.

Electron heat flow is commonly treated as being due to a small disturbance $\mu f_1$ of an otherwise Maxwellian velocity distribution $f_M$ of the electrons [2, 3]:

$$f_e(s, w, \mu) = f_o(s, w) + \mu f_1(s, w) \tag{2.1}$$

where

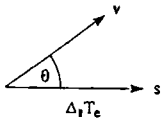


$$w = \frac{1}{2} m_e v^2 - e\phi(s), \quad \mu = cos\ \theta \tag{2.2}$$

$$f_o = f_M = n_e \left(\frac{m_e}{2\pi T_e}\right)^{3/2} e^{-(w+e\phi)/T_e}. \tag{2.3}$$

$n_e(s), T_e(s)$ and $\phi(s)$ are electron density, temperature and electric potential at distance s along $\underline{B}$. Putting this ansatz into the Fokker-Planck equation (for ions at rest)

$$\mu v \frac{\partial f_e}{\partial s} + \frac{e}{m_e}\frac{\partial \phi}{\partial s}(1-\mu^2)/v \frac{\partial f_e}{\partial \mu} = C_{ei} + C_{ee} = \frac{v}{\lambda_{ei}}\frac{\partial}{\partial \mu}(1-\mu^2)\frac{\partial f_e}{\partial \mu} + C_{ee} \tag{2.4}$$

where $C_{ei}$ and $C_{ee}$ are the electron-ion and electron-electron collision terms and assuming $C_{ei}$ dominant as compared to $C_{ee}$ one gets the solution

$$f_1 = -\frac{1}{2}\lambda_d \frac{\partial f_M}{\partial s} \tag{2.5}$$

where $\lambda_d(v) \propto v^4$ is the electron mean free path length for 90° deflection by electron-ion and electron-electron collisions. $\partial f_M/\partial x$ is a function of $v/v_{te}$, and is linear in the derivatives $n_e'/n_e, T_e'/T_e$ and $e\phi'/T_e$ with $' = \partial/\partial s, v_{te} = (T_e/m_e)^{1/2}$.

The first and third order moments of $f_e$ give equations for the electron momentum flux $\Gamma_e$ (Ohm's law)

$$\Gamma_e = \frac{4\pi}{3}\int_o^\infty dv\ v^3 f_1 \tag{2.6}$$

and electron heat flux

$$q_e = \frac{2\pi}{3} m_e \int_o^\infty dv\ v^5 f_1 \tag{2.7}$$

including the thermoelectric effects.

Eliminating $\phi'$ by equ. (2.6), $q_e$ becomes a linear function of $T_e'$ and electric current. For zero current, $\Gamma_e = 0, q_e$ is given by [3]

$$q_e = n_e v_{te} \lambda_e T_e' \int_0^\infty g(v/v_{te}) d(v/v_{te}) = 3.2 n_e v_{te} \lambda_e T_e', \quad \lambda_e = \lambda_d(v_{te}) = v_{te}\tau_e \tag{2.8}$$

The contribution to the heat flux $g(v/v_{te})$ by electrons of different velocities $v$ is plotted in Fig. 2. It can be seen, that most of the contribution comes from electrons with $v_{hc} \sim 3...5 v_{te}$, i.e. with an energy of $\sim 10 T_e$.

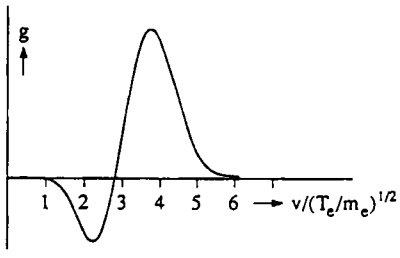


Fig. 2: *Contribution of electrons with different velocities v to the heat flux $q_e$*

In order to be consistent with the assumption of $f_1 \ll f_M$ the heat flux carrying electrons must have mean free path lengths less than the temperature gradient length,

$$\lambda_d(v_{hc}) T_e'/T_e < 1. \tag{2.9}$$

From this condition follows for $\lambda_e$

$$\lambda_e T_e'/T_e \lesssim 10^{-2} \tag{2.10}$$

and

$$q_e \lesssim 3.10^{-2} n_e v_{te} T_e \tag{2.11}$$

## 2.2 Fokker-Planck modelling of the Electron Heat Flux in the SOL.

How far are the conditions of local heat conduction fulfilled in the SOL?
At the sheath edge the electron heat flux is determined by the properties of the sheath to be [4]

$$q_{es} = (\delta_e - \frac{\gamma_e}{\gamma_e - 1}) n_{es} V_s T_{es} \gtrsim \left(\delta_e - \frac{\gamma_e}{\gamma_e - 1}\right) \frac{\gamma_i T_{is} + T_{es}}{T_{es}} (\frac{m_e}{m_i})^{1/2} n_{es} v_{tes} T_{es} \sim 0.1 n_{es} v_{tes} T_{es} \tag{2.12}$$

where $V_s$ and $T_s$ are flow velocity and temperatures at the sheath edge, $\gamma$ the adiabatic constant and $\delta_e \sim 5$.
Thus, the condition for applicability of the Braginskii heat conductivity is marginally violated near the sheath edge.
Its applicability to other parts of the SOL were checked by comparison with results from a kinetic Fokker-Planck particle code [1]. This code includes Coulomb collisions as well as sheath effects. (The length scale of the latter are artificially enlarged but still small as compared to all other length scales in the system.)

Two cases are considered:
a) A source S of hot electrons and ions near the midplane and a completely absorbing target (Fig. 3a).
b) A completely recycling target, i.e. a source of cold recycled electrons and ions in front of the target proportional to the particle flux impinging on the target (Fig. 3b).
In both cases the heat flux from the core is modelled by a fixed temperature $T_o$ which all particles assume when passing (being reflected at) the symmetry plane at $x = 0$.

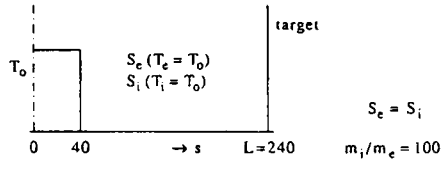


Fig. 3a: *Hot particle source remote from the target (Case a)*

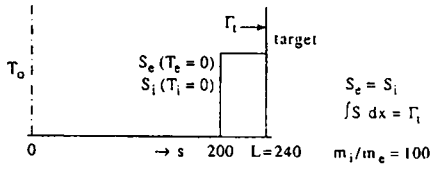


Fig. 3b: *Cold recycling particles at the target (Case b)*

Case a) Remote Source.
Fig. 4 shows profiles of electron temperature $T_e$ heat flux $q_e$ and meanfree path length $\lambda$ for two collisionalities labeled by $\lambda_o$, the electron mean free path length at temperature $T_o$,

$$\lambda_o = \lambda_e(v = (T_o/m_e)^{1/2}). \tag{2.13}$$

The temperature profiles in both cases are rather flat.

For $\lambda_o = 38$ the heat flux $q_e$ has a flat minimum. The mean free path length at this minimum is $\lambda_e \sim 16$ (compared to a system length L = 240) and the gradient length $T_e/T_e' \sim 710$ such that $\lambda_e T_e'/T_e \sim 2.3 \cdot 10^{-2}$. The $T_e$ profile by integrating the relation $T_e' = -q_e/\kappa_e$ with $\kappa_e$ the Braginskii heat conductivity is shown for comparison and differs not too much from the F.P. result for $T_e$.
For $\lambda_o = 380$ the mean free path length $\lambda_e \sim 180$ and $\lambda_e T_e'/T_e \sim 1.7$, i.e. the plasma is nearly collisionless. Nevertheless, the electron velocity distribution stays nearly Maxwellian if the source is Maxwellian. $q_e$ in this case is nearly constant in $x$ between the source and sheath regions and completely determined by the boundary condition (2.12) at the sheath.

Fig. 5 shows for different collisionalities $\lambda_o/L$ the electron heat flux $q_e$ from the F.P. model and from integration of the local heat conduction equation $q_e = -\kappa_e T_e'$ with boundary conditions $T_e = T_o$ at $s = 0$ and (2.12) at $s = L$. As may be seen there are only slight differences at intermediate values of $\lambda_o/L$. For large values of this parameter the value of $q_e$ is determined by the boundary condition (2.12) likewise in both models [5].

Case b) Recycling Source.
The situation completely changes if there is a source of cold recycling particles just in front of the target. The recycling coefficient is assumed to be $R = 1$ and the initial temperature of the recycled ions and electrons to be zero. Again the heat flux from the core is assumed to maintain a constant midplane tempera- $T_o$ for passing particles.
Profiles of density, temperatures, potential and heat flux together with the mean free path length $\lambda$ are shown in Fig. 6. The density shows a strong increase, the ion and electron temperatures a strong decrease in the recycling region due to the admixture of cold particles. But also outside the recycling region the temperature gradients are rather large, i.e. $\lambda_e T_e'/T_e \sim 0.17$ and 11.8 at the midplane $s = 0$ for $\lambda_o = 38$ and 380 respectively. Here the Braginskii heat conductivity completely fails to describe the relation between electron heat flux and temperature even for the higher collisionality $\lambda_o = 38$.
The potential $\phi$ shows a local maximum for $\lambda_o = 38$ at the edge of the recycling zone and is

Electron heat flux

Remote source

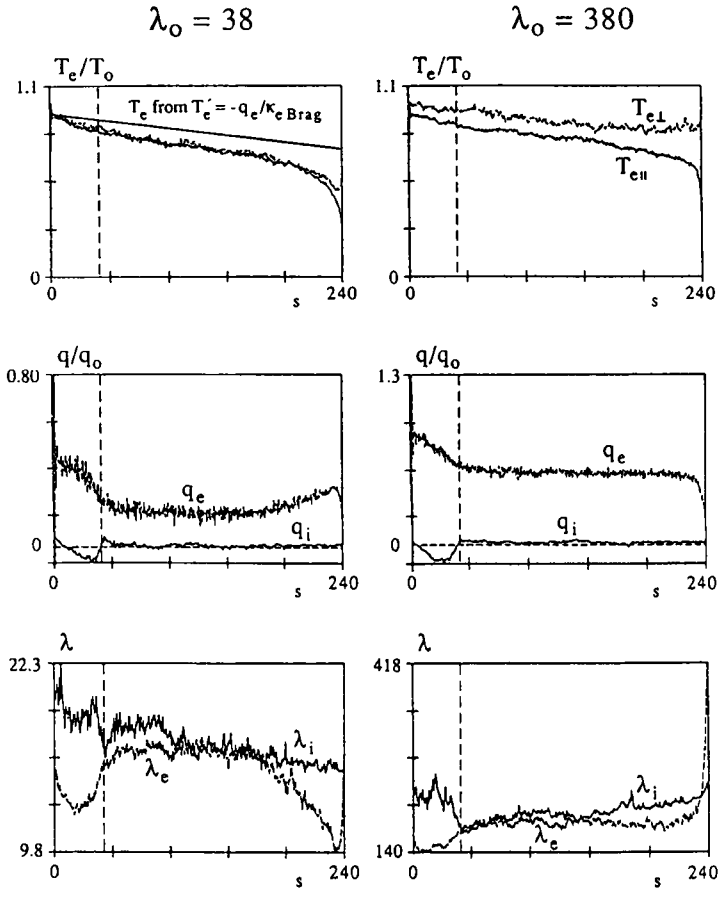


Fig. 4: *Electron temperature and heat flux for case a*

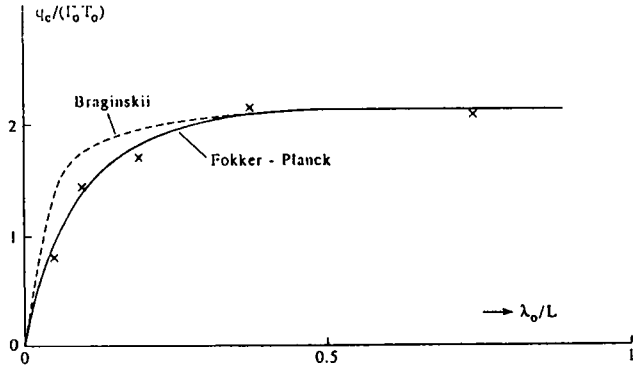


Fig. 5: *Electron heat flux as function of mean free path length $\lambda_o$ for case a*

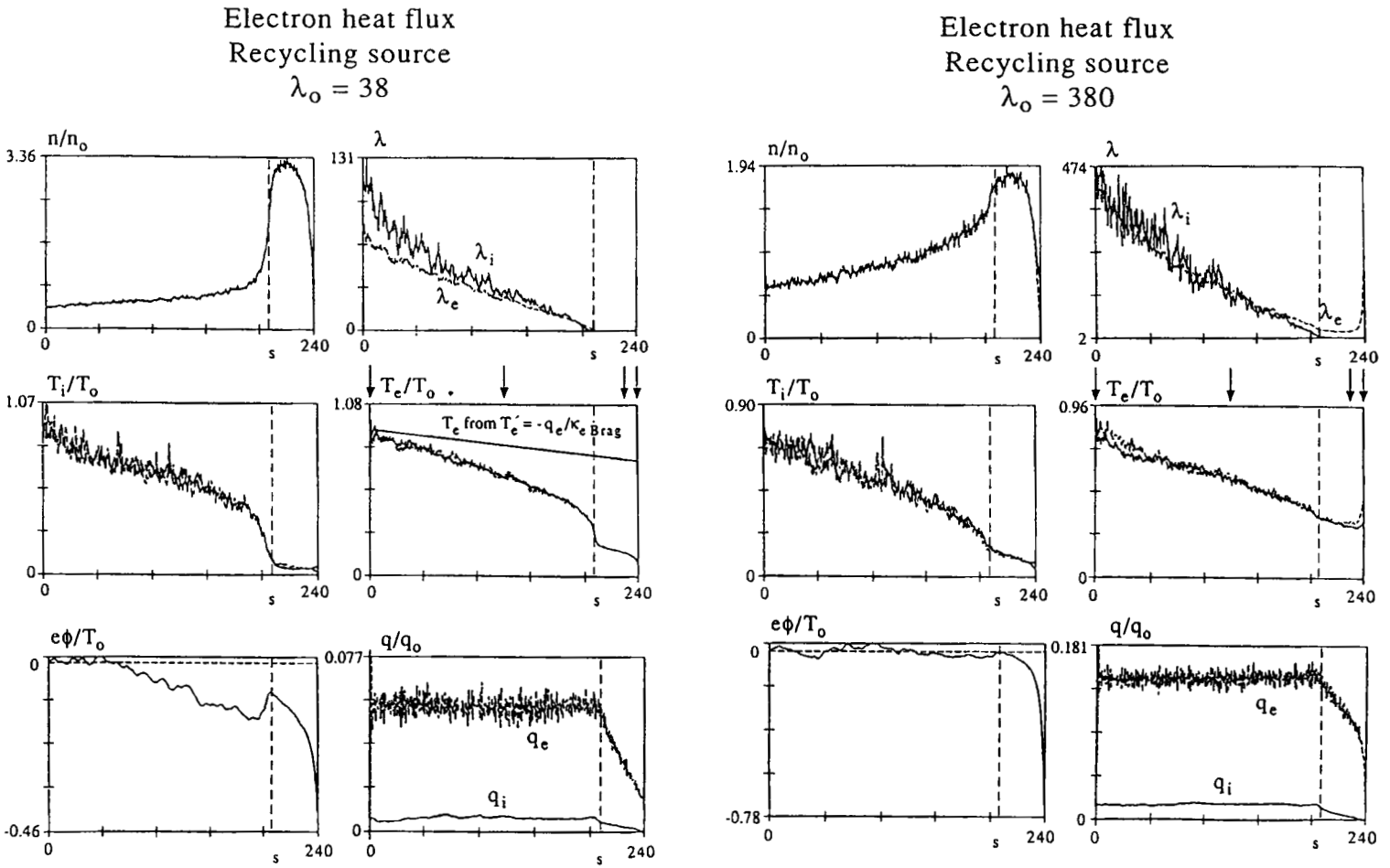


Fig. 6: *Electron temperature and heat flux for case b*

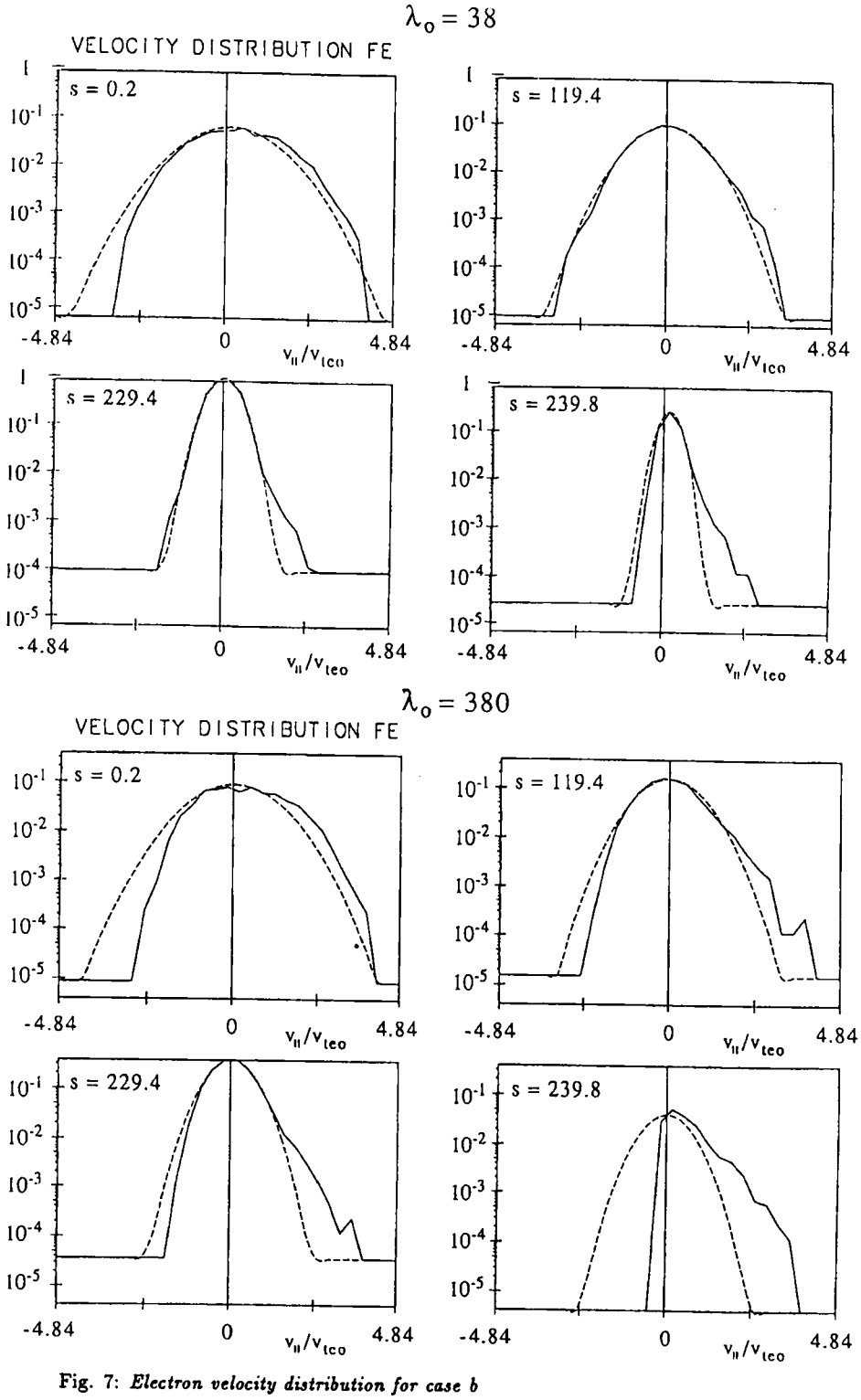


Fig. 7: *Electron velocity distribution for case b*

rather flat for $\lambda_o = 380$. The potential drop between midplane and target rises with increasing mean free path length $\lambda_o$. This is due to the fact that with increasing $\lambda_o$ hot particles from the midplane reach the target without collisions. Thus the sheath potential more and more adjusts itself to the hot midplane temperature rather than to the cold local temperature at the sheath edge.
This mixing effect of hot midplane and cold recycling particles is shown in Fig. 7 by the velocity distributions of electrons at different locations (indicated by arrows in Fig. 6): The velocity distribution in the recycling zone is composed of a Maxwellian part (dashed line) of relatively cold particles resulting from collisions between cold recycled and hot midplane particles and of a small part of hot midplane particles transversing the recycling zone without collisions. Thus the velocity distribution of plasma particles in this case become non-Maxwellian and the heat flux results from a non-local response to the temperature profile.

2.3 Non Local Electron Heat Conduction Theory.

Non local heat transport of electrons down steep temperature gradients have been studied extensively both numerically and analytically and several attempts have been made to incorporate it into fluid models, mainly in connection with laser-target interaction [6 – 10]. I would like to quote one of them [11, 12] in more detail because it is a direct and lucid extension of the local theory.
The supposition of this approach is that the electron deflection length $\lambda_d$ is much smaller than the length for energy loss of superthermal electrons $\lambda_w$. Accordingly the evolution of the electron velocity distribution takes place at two length scales: short scale isotropization by collisions with ions and electrons and long scale Maxwellization by electron-electron collisions. The perturbation ansatz at the short scale is as before

$$f_e(s,w) = f_o(s,w) + \mu f_1(s,w) \tag{2.14}$$

but now $f_o$ is assumed to be only isotropic, not necessarily Maxwellian. Then, as in equ. (2.5)

$$f_1 = -\frac{\lambda_d}{2}\frac{\partial f_o}{\partial s} \tag{2.15}$$

where $\lambda_d(v)$ is the electron path length for deflection.

The approach of $f_o$ to a Maxwellian distribution is given by the second order equation

$$\frac{1}{3v}\frac{\partial}{\partial s}(v^2 f_1) = C_{ee}(f_o - f_M, f_o) = \frac{2m_e v^3}{\lambda_w}\frac{\partial}{\partial w}(f_o - f_M) \tag{2.16}$$

with $\lambda_w(v)$ the path length for energy loss of the superthermal electrons. The solution gives $f_o$ as a linear functional of $f_M$.

Knowing $f_o$ and therefore $f_1$ one can again derive electron momentum and heat flux equations of the form

$$\Gamma_e = K_{11}(T_e'/T_e) - K_{12}(e\phi^{*\prime}/T_e) \tag{2.17}$$

and

$$q_e = K_{21}(T_e') - K_{22}(e\phi^{*\prime}) \tag{2.18}$$

with

$$e\phi^{*\prime} = e\phi' - T_e n_e'/n_e + 5/2T_e'. \tag{2.19}$$

The K's are linear functionals of their arguments

$$K(h(s)) \propto \lambda_s/\lambda_w \int ds' n_e(s') v_{te}(s') P(\Theta(s,s'))h(s') \tag{2.20}$$

where

$$\Theta(s,s') = |\int_s^{s'} ds'' n(s'')/(n(s')\lambda_s(s'))| \sim |s-s'|/\lambda_s(s') \tag{2.21}$$

with

$$\lambda_s = (\lambda_d(v_{te})\lambda_w(v_{te}))^{1/2} \tag{2.22}$$

is the so-called stopping length and P(Θ) for large Θ falls off exponentially in $\Theta^{2/5}$.
Equs. (2.17) and (2.18) give the non-local relations between gradients of electron temperature and potential on one side and electric current and electron heat flux on the other. In order to get $q_e$ as a functional of $T_e'$ and current $\Gamma_e$ one has to invert equ. (2.17) and eliminate $\phi^{*\prime}$.

## 3. Ion Viscosity along B

Ion viscosity $\Pi_{i\|}$ parallel to B is defined by the anisotropy of the pressure tensor

$$\Pi_{i\|} \equiv \frac{2}{3}(p_{i\|} - p_{i\perp}) \tag{3.1}$$

Local transport theory gives a relation between $\Pi_{i\|}$ and the change of the flow velocity $V$ along B[3].

$$\Pi_{i\|} = -\mu \frac{\partial V}{\partial s}. \tag{3.2}$$

As for the electron heat flux there may be a deviation from this relation due to large ion mean free path lengths compared to the length of change of $V_i$.
In Fig. 8 numerical examples are shown for two flow states according to case a and b of the section 2.2 (remote and recycling sources). Viscosity builds up in the source region where V is rising. For the recycling source, ion temperature and mean free path length $\lambda_i$ are small and the viscosity stays negligible. For the remote source $\lambda_i$ becomes comparable or larger than the source extension $d = 40$. $\Pi_{i\|}$ becomes noticeable and may persist during the sourceless flow to the target in contrast to equ. (3.2). This is due to the lack of collisions which cannot transfer energy from perpendicular degrees of freedom into the parallel expansion flow. Therefore the pressure stays anisotropic. $p_{i\|}$ may be described in a nearly collisionless fluid by an adiabatic constant $\gamma_i \sim 3$ rather than by $\gamma_i = 5/3$ and equ. (3.2).

## 4. Sheath

In front of a charge neutralising target a thin sheath of negative potential is formed which reflects most of the incoming electrons. With a magnetic field oblique to the target the sheath potential exhibits two length scales, the ion gyroradius and the Debye length [13]. For increasing angle $\psi$ between magnetic field and target normal the potential drop at the gyroscale increases, the drop at the Debye scale decreases while the total potential difference across the sheath stays nearly constant. At a critical angle which depends on mass and temperature ratio of ion and electrons and is of the order $90° - \psi \sim 1°$ the potential change over the Debye scale becomes zero. For still larger angles $\psi \to 90°$ it becomes positive because ions then tend to move faster to the target than electrons [14]. Above this critical angle the total potential difference across the sheath decreases. Electrons reflected from the target also reduce the potential difference across the sheath. The reduction vanishes for $\alpha \to \alpha_{crit}$.

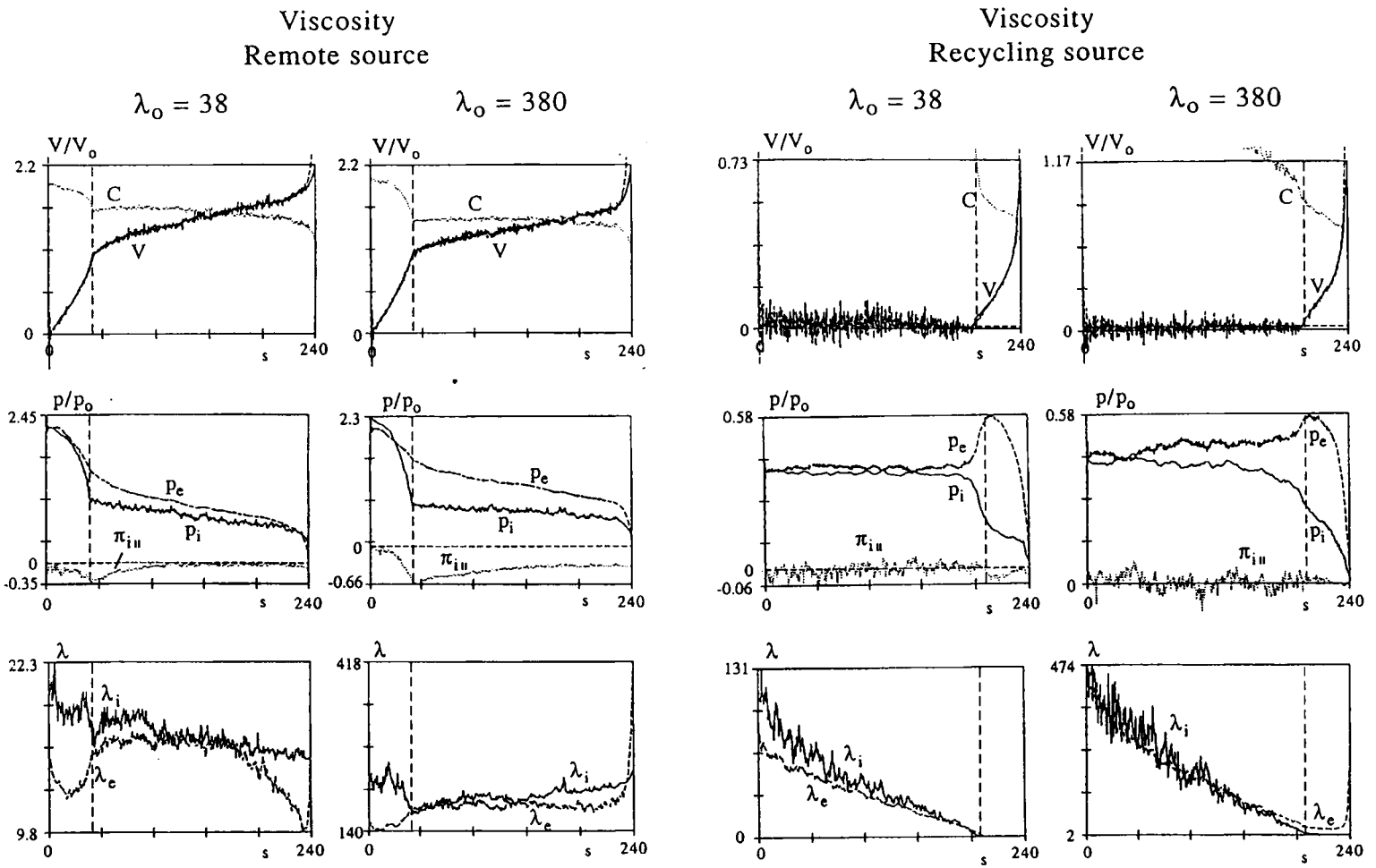


Fig. 8: *Flow velocity and viscosity for case a and b*

## 5. Boundary Conditions

One of the advantages of a kinetic model of the SOL is the possibility to pose clear boundary conditions right at the target plate. A fluid model on the other hand has to exclude the sheath region just in front of the target because the suppositions for the fluid description are violated there (Fig. 9). Therefore kinetic considerations must close the gap between fluid boundary and target.

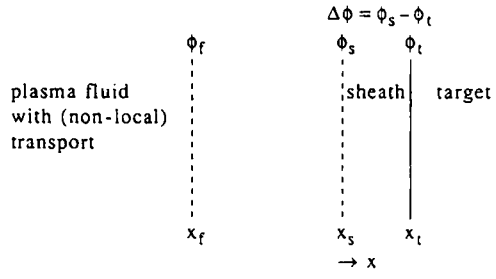


Fig. 9: *Location of fluid boundary*

### 5.1 Electron Heat Flux

There is a rather clear boundary condition for the electron heat flux: Due to high energy electrons which have not been reflected by the sheath the electron distribution at the sheath edge has a cut (Fig. 10). This cut gives rise to a heat flux $q_e = [\delta_e - \gamma_e/(\gamma_e - 1)]n_e V_e T_e$ at $x_s$ and approximately also at $x_f$ where $\delta_e \sim 2 + e\Delta\phi/T_e$ and $\Delta\phi$ is the potential difference across the sheath. A difficulty arises for matching the nonlocal heat flux described in section 2.3 to this boundary condition. One has to find such an electron temperature profile that the isotropic part of the electron distribution function $f_o$ (which is a functional of this profile) in its truncated form (Fig. 10) just gives the boundary heat flux $q_e(x_f)$ quoted above.

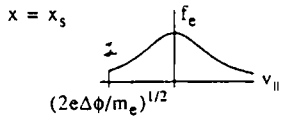


Fig. 10: *Truncated electron velocity distribution at the sheath edge.*

An other procedure is proposed in [15] using an analytic solution of the kinetic equation for the electron distribution function with the boundary condition of Fig. 10 but assuming a Krook collision operator.

### 5.2 Ion Flow Velocity, Viscosity and Heat Flux

Assuming a totally absorbing target and negative sheath potential the ion distribution function at the fluid boundary is not at all affected by the sheath and the target and determined only by the upstream conditions (sources, transport etc.). Therefore no boundary conditions can be posed on the ion fluid at the target.
The Bohm relation, $V \geq C_s$ at the boundary, should be fulfilled of its own. If dissipation processes as viscosity and heat conduction are included in the fluid model they should be treated as small corrections and be determined iteratively from velocity and tempterature profiles of the previous iteration cycle in order to avoid the need for boundary conditions.

## 6. Summary

In case of strong target recycling the electron temperature drop along the SOL from the midplane to the target is larger than that calculated from Braginskii heat conductivity. Fluid codes, therefore, should take into account the nonlocal dependence of parallel electron thermoforce and heat flux on the temperature gradient $\nabla_{||} T_e$.

Ion viscosity may become appreciable in cases of no recycling where temperatures and mean free path length as compared to gradient length are larger than in the recycling case. It may be accounted for by using an adiabatic constant $\gamma_i \to 3$ instead of 5/3.

For small electron gyro radii as compared to the Debye length and particle flow purely parallel to a magnetic field with grazing incidence angle $\alpha < \alpha_{crit} \sim 1^0$ on the target plane, the sheath potential exhibits a minimum i.e. the sheath becomes a double layer of negative and positive net charge. The potential drop across the sheath in this case becomes smaller and may even reverse its sign.

Secondary electrons reflected from the target with low energies reduce the potential drop across the sheath. The reduction tends to zero for $\alpha \to \alpha_{crit}$.

Fluid boundary conditions on the electron heat flux should take into account the non local dependence on the temperature gradient and the reflection conditions at the sheath. At a particle absorbing target no boundary conditions should be posed on ion flow velocity, viscosity and heat flux.

## References


[1] R. CHODURA, 8$^{th}$ Europ. Conf. on Comp. Physics, Eibsee, 1986, Europhysics Conf. Abstracts, Vol. 10D, 97

[2] L. SPITZER, R. HÄRM, Phys. Rev. 89, 977 (1953)

[3] S.I. BRAGINSKII, in Reviews of Plasma Physics, Vol. 1, M.A. LEONTOVICH ed., Consultants, New York, 1965

[4] R. CHODURA, in Physics of Plasma Wall Interactions in Controlled Fusion, D.E. POST, R. BEHRISCH eds., Plenum Press, New York, 1986

[5] R. CHODURA, 13$^{th}$ Europ. Conf. on Controlled Fusion and Plasma Heating, Schliersee, 1986, Europhysics Conf. Abstracts, Vol. 10C, part 1, 411

[6] A.R. BELL, R.G. EVANS, D.I. NICHOLAS, Phys. Rev. Lett. 46, 243 (1981)

[7] R.J. MASON, Phys. Rev. Lett. 47, 652 (1981)

[8] S.A. KHAN, T.D. ROGNLIEN, Phys. Fluids 24, 1442 (1981)

[9] J.P. MATTE, J. VIRMONT, Phys. Rev. Lett. 49, 1936 (1982)

[10] Yu.L. IGITKHANOV, P.N. YUSHMANOV, Contrib. Plasma Phys. 28, 341 (1988)

[11] J.R. ALBRITTON, E.A. WILLIAMS, I.B. BERNSTEIN, K.P. SWARTZ, Phys. Rev. Lett. 57, 1887 (1986)

[12] F. MINOTTI, C. FERRO FONTAN, Phys. Fluids B2, 1725 (1990)

[13] R. CHODURA, Phys. Fluids 25, 1628 (1982)

[14] R. CHODURA, 19$^{th}$ Europ. Conf. on Controlled Fusion and Plasma Physics, Innsbruck, 1992, Europhysics Conf. Abstracts Vol. 16, part 2, 871

[15] Y.L. IGITKHANOV, A.M. RUNOV, this workshop